PNAS RESEARCH ARTICLE | NEUROSCIENCE

# Neural network architecture of a mammalian brain

Larry W. Swanson[a,1], Joel D. Hahn[a], and Olaf Sporns[b,c]

Affiliations are included on p. 11.

Contributed by Larry W. Swanson; received July 4, 2024; accepted August 14, 2024; reviewed by Ann M. Graybiel and Liqun Luo

**Connectomics research is making rapid advances, although models revealing general principles of connectional architecture are far from complete. Our analysis of $10^6$ published connection reports indicates that the adult rat brain interregional connectome has about 76,940 of a possible 623,310 axonal connections between its 790 gray matter regions mapped in a reference atlas, equating to a network density of 12.3%. We examined the sexually dimorphic network using multiresolution consensus clustering that generated a nested hierarchy of interconnected modules/subsystems with three first-order modules and 157 terminal modules in females. Top–down hierarchy analysis suggests a mirror-image primary module pair in the central nervous system's rostral sector (forebrain–midbrain) associated with behavior control, and a single primary module in the intermediate sector (rhombicbrain) associated with behavior execution; the implications of these results are considered in relation to brain development and evolution. Bottom–up hierarchy analysis reveals known and unfamiliar modules suggesting strong experimentally testable hypotheses. Global network analyses indicate that all hubs are in the rostral module pair, a rich club extends through all three primary modules, and the network exhibits small-world attributes. Simulated lesions of all regions individually enabled ranking their impact on global network organization, and the visual path from the retina was used as a specific example, including the effects of cyclic connection weight changes from the endogenous circadian rhythm generator, suprachiasmatic nucleus. This study elucidates principles of interregional neuronal network architecture for a mammalian brain and suggests a strategy for modeling dynamic structural connectivity.**

cluster analysis | connectomics | hubs | modules | subsystems

## Significance

The adult brain's internal wiring diagram was analyzed using network science methods for a common laboratory mammal (rat). Unsupervised cluster analysis generated a hierarchical model of interconnected modules or subsystems aligning more with evolutionarily conserved developmental compartments than with current functional system parcellation and categorization. Focal computational manipulations identify which regions have the most effect on global network organization, reveal possible factors underlying these effects, and model the influence of circadian rhythms. In this dynamic structural connectivity model, the effects of local changes in connection strength tend to express within modules, suggesting the testable hypothesis that normal physiological and pathological changes spread preferentially through modules.

The brain is to the nervous system as the heart is to the circulatory system. To understand the circulatory system's basic plan, it was important to know the heart's internal organization as a double pump for blood coursing through arteries, capillaries, and veins. To understand the nervous system's basic plan, it will be important to clarify the intrinsic organization of the brain's neural network, as a controller and coordinator of behavior and homeostasis via the spinal cord, peripheral nervous system, and pituitary gland. One goal of this quest is to evolve for systems neuroscience a rigorous conceptual framework like chemistry's periodic table of elements or molecular biology's double helix model of DNA. Recently, network science has provided mathematical tools for generating quantitative, systematic, unsupervised, and global insights into the basic organizing principles of the nervous system's wiring diagram based on a connectome (1).

The general strategy for successfully reverse engineering any complex system or network, especially one comparable to the nervous system, involves three basic steps (2, 3). First, the analysis should be guided by an understanding of the system's main functions. Second, it is important to have a global parts list, to understand how each part works, and to model how those parts connect causally as a functional system. And third, it is practical and instructive to start with a high-level plan of the architecture and then cycle through step two toward successively finer granularity levels.

Based on these three principles, we are developing a strategy to clarify the neural network architecture of a common laboratory mammal, the rat (4–17). One basic component of this strategy is a global nested hierarchy of nervous system gray matter parts (Fig. 1) with divisions at the upper, large-scale levels, followed by nested gray matter regions in the middle, and two bottom levels with nested neuron types and then nested individual neurons (5, 18–20). In such a nested hierarchy, neural processing via connections between parts at any level of interest is influenced by processing at lower levels, and processing in that level of interest influences processing in the levels above it, where emergent properties occur (21). Thus, no level acts in isolation, and no level is privileged over others (22).

The level with gray matter regions and axonal connections between them (hereafter simply called regions and connections, respectively) was chosen for our analysis of nervous system neural network organization—dealing in this paper with the brain's internal

Author contributions: L.W.S., J.D.H., and O.S. designed research; L.W.S. and J.D.H. performed research; L.W.S., J.D.H., and O.S. analyzed data; L.W.S. wrote first draft of the paper; J.D.H. substantial revisions of first draft; O.S. additional revisions of first draft; and L.W.S. wrote the paper.

Reviewers: L.L., Stanford University; and A.M.G., Massachusetts Institute of Technology.

The authors declare no competing interest.



[1]To whom correspondence may be addressed. Email: larryswanson10@gmail.com.

This article contains supporting information online at https://www.pnas.org/lookup/suppl/doi:10.1073/pnas.2413422121/-/DCSupplemental.

Published September 17, 2024.

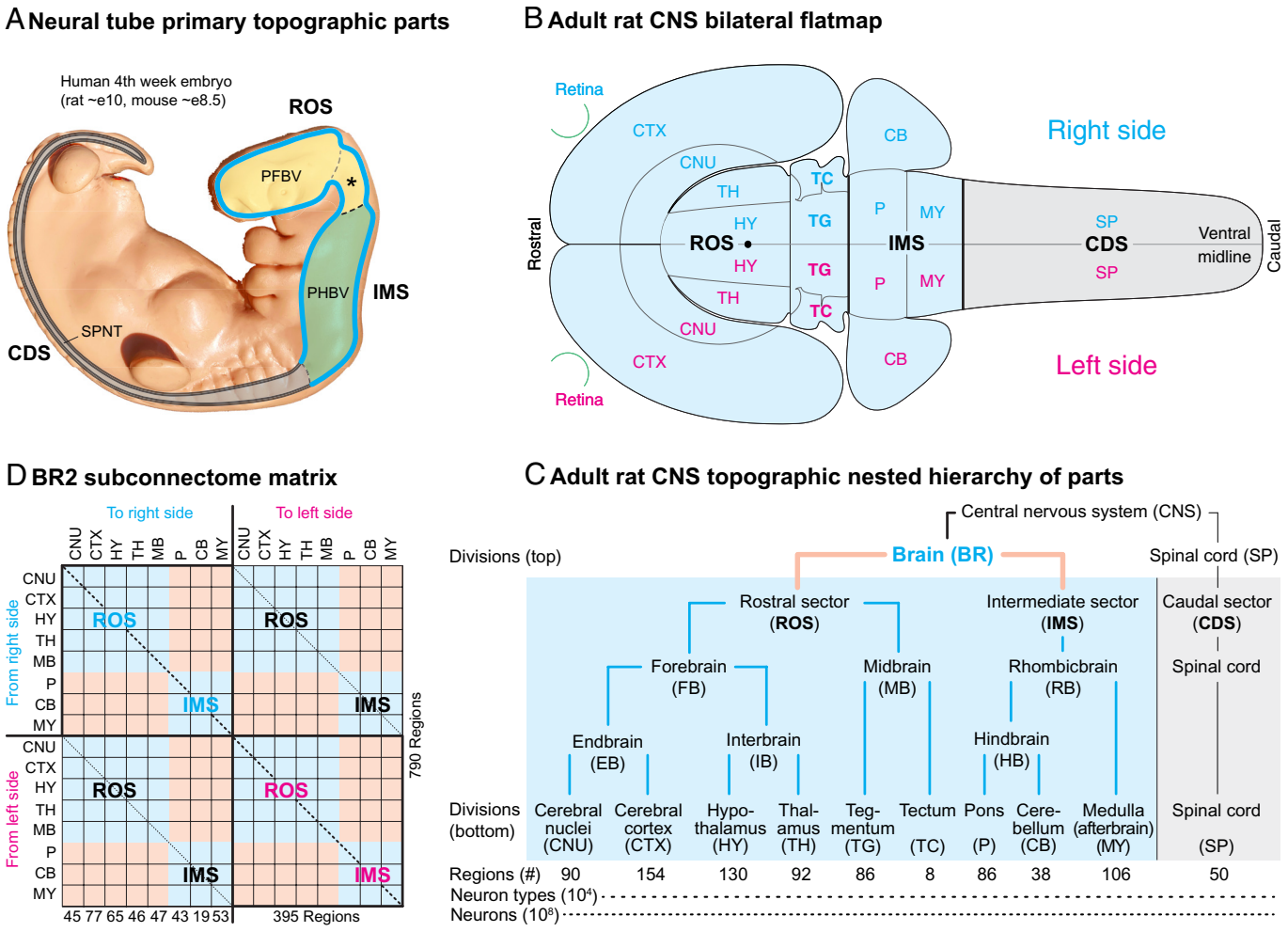


**Fig. 1.** A nested hierarchy of central nervous system (CNS) parts for connectomics studies in chordates and applied here to a mammalian (rat) brain. (*A*) Topographic parts description is based on neural tube development that early on presents three sectors: rostral (ROS), intermediate (IMS), and caudal (CDS). Soon the ROS splits into primary forebrain vesicle (PFBV) and primary midbrain vesicle (indicated by an asterisk), the IMS is the primary hindbrain vesicle (PHBV), and the CDS is the spinal cord part of neural tube (SPNT); shown superimposed schematically on a human embryo model. (*B*) The neural tube's brain segment eventually generates 9 major bilateral divisions, shown for adult rat (light blue) on a flatmap shaped like the embryonic neural plate (23). (*C*) Topographically arranged, nested hierarchy of major CNS parts (with abbreviations) common to adult chordates, as represented here for the rat, specifically. Gray matter regions are a nested level below the nine major bottom-level divisions in (*B*), neuron types are a nested level below regions, and individual neurons are a nested level below neuron types. (*D*) A matrix of subconnectomes for nine major bottom-level brain divisions (tegmentum and tectum are combined into midbrain); subconnectomes published previously for the ROS (15) and IMS (16) are shaded light blue, those for connections between ROS and IMS, and collated for this paper, are colored light red (same color scheme as in *C*) (Adapted from ref. 16). Connectome versioning is necessary to accommodate future revisions, as when new data appear (9); its occurrence here is documented in Dataset S2. The main diagonal (dashed line from *Upper-Left* to *Lower-Right*) passes through subconnectomes with ipsilateral intradivisional connections; two shorter parallel secondary diagonals indicate subconnectomes with contralateral intradivisional connections.

connectivity. This intermediate network level of interregional connections is species-specific and genetically determined during development (6), unlike the refined lower levels that are specific for individuals and continually modified dynamically from the intermediate connectivity pattern (24). Our region-level neuroanatomically founded approach stands in contrast to earlier mouse brain subregional voxel-based connectome models with less brain-wide coverage (25, 26).

Our analysis is based on systematically collated and curated axonal transport connectivity tracing experimental data from the neuroanatomical literature, and is supported by an open-access neuroanatomical reference atlas of rat brain gray matter regions (27), an evolving neuroanatomical universal reference ontology of defined terms for nervous system parts (22, 27, 28), and a defined vocabulary for describing axonal connections (18). This information was used to construct a database of intrinsic brain connections for all rat brain regions, including an assessment of whether each possible connection exists, and if so a qualitative assessment of its maximum weight. The connectome database was then represented numerically as a matrix of weighted and directed axonal connections for computational analysis using a suite of basic mathematical-statistical network science methods for detecting locally dense network connectivity (using cluster analysis), global network features (based on region centrality), and the effect of local connection weight changes on network organization (by computational manipulation of the network). The results provide a framework for a conceptual structure–function model, and a foundational resource for an open-access brain connectivity knowledge management system.

## Results

Our general strategy for constructing, analyzing, interpreting, and computationally manipulating a connectome is presented here, applied specifically to the intrinsic connectivity of the adult bilateral brain network (BR2; related abbreviations: BR2f, adult bilateral female brain network; BR2m, adult bilateral male brain network).

**A Brain Connectome Foundational Database from 50 y of Research.** An obligatory first step was creation of a connection database. It was collated primarily from the results of experimental axonal transport pathway tracing studies (adopted since 1973) indicating the presence and weight, or the absence, of from–to (directed) axonal connections between all 790 regions/nodes on the right (395 regions) and left (395 corresponding regions) sides of the adult rat brain in our reference nomenclature hierarchy and spatial atlas (for a complete account of collation strategy see *SI Appendix*, *Materials and Methods*; for brain part abbreviations, see Dataset S1). This fully annotated nomenclature and atlas has been under constant revision since 1974 and is now in its fourth edition (27). The region level was chosen for analysis because currently it is the deepest granularity level with enough available data to assemble a systematic and reasonably complete connection matrix for a mammalian brain. For example, a connection matrix for brain neuron types (the next deepest granularity level) may require about two orders of magnitude more data (Fig. 1*C*).

Connection reports, ranging from none to 12 (mean of 1.66, mode of 2) for connections arising on one side (doubled for both sides to 24 maximum, mean of 3.32, and mode of 4), for each possible connection in the connection matrix were expertly collated by L.W.S. (97.0%) and J.D.H. (3.0%) from the primary structural neuroscience literature. This information was recorded in a conditionally formatted Excel worksheet (AxiomeM3.21, designed by J.D.H.; Dataset S2) with ≥18 columns of data and metadata per report; for a comparison of collation results for the same connection matrix by two experts see ref. 8. By using a nested parts hierarchy, axonal connection data at region, neuron type, and individual neuron analysis levels were aggregated in the database (Fig. 1*C*).

**Basic Brain Connectome Properties Reveal a Sparse Network (Fig. 2).** No statistically significant left–right or strain differences were identified during our systematic collation. Thus, all ipsilateral and contralateral connections were assigned to one side of the brain, and the same dataset was employed for the other side. However, two left–right pairs of clearly sexually dimorphic connections were identified, requiring separate analysis of the genetically female and male brain neural networks of *Rattus norvegicus domestica*.

The full dataset has 1,034,078 connection reports for 623,310 possible BR2 connections. These data were collated from 1,472 original research publications appearing in 121 journals, books, or theses since 1973; 50.9% of the reports were from the *Journal of Comparative Neurology*. The data were generated employing 41 different axonal transport pathway tracing methods; L.W.S. lab and principal coauthored publications provided the largest share of connection reports (19.3% of the full set, and 25.0% of those selected for network analysis).

Our collation identified 72,324 connections that exist (are present) in the BR2 network, and 513,588 connections that do not exist (are absent), giving a relatively sparse network connection density of 12.3%. No data were found for 6.0% of all possible connections (a connectome fill ratio of 94.0%); accordingly, based on a connectivity density of 12.3% for available data, we estimate the BR2 network contains about 76,940 connections. During collation, existing connections were assigned a weight based on an ordinal scale (Fig. 3, *First* column; Datasets S3 and S4, Layer E) because a scarcity of relevant quantitative data precluded its general use.

Remarkably, the data suggest that on average a brain region projects directly to (and receives projections directly from) 92 other brain regions. For individual regions, out of a possible 789 connections (excluding self-connections), the range of BR2 output connections is 0 to 494 and the range of input connections is 2 to 357; when combined, the range of total inputs + outputs for individual BR2 regions is 5 to 649 (out of 1,578).

For network analysis, values of connection weight recorded as "no data" were binned with absent and unclear values (Fig. 3, *Second* column; Datasets S3 and S4, Layer F). Then, the descriptive ordinal scale was converted to a more realistic connection weight scale covering the reported range of 5 orders of magnitude in connection density for rat connectional data (6) (Fig. 3, *Third* column; Datasets S3 and S4, layer G).

Last, a validity metric based on a 7-point ordinal scale (1 to 7: lowest-highest validity) was applied to the axonal pathway tracing method associated with the connection report for each connection in the connectome (13, 14) (Dataset S4, Layer I). This metric is based on three criteria: the method's reach (monosynaptic preferred over polyneuronal), sensitivity, and possible involvement of axons-of-passage. The following average validity values were determined for the data used for BR2 network analysis: for connections reported to exist, ipsilateral (within one side) = 6.32, contralateral (between sides) = 6.20, both sides = 6.28 (for the 72,324 connections indicated to exist); for connections reported to not exist, ipsilateral = 6.00, contralateral = 6.02, both sides = 6.01 (for the 513,588 connections indicated to not exist).

**Structure–Function Module Analysis Using MRCC.** After creating and summarizing a foundational structural database, we examined with quantitative network science tools possible local (subglobal),

| Measure / Major CNS part | Regions (nodes) [1] | Connections possible [2] | | Connections present [3] | | Completeness of dataset [4] (%) | Connection density [5] (%) | Connection reports [6] |
|---|---|---|---|---|---|---|---|---|
| | | data available | total | data available | extrapolated | | | |
| Brain | 790 | 585,912 | 623,310 | 72,324 | 76,940 | 94.0 | 12.3 | 1,034,078 |

[1] Number of regions (nodes) on right and left side of the brain (sides are regarded as symmetrical in this analysis).

[2] Number of possible connections (bilateral): data available (column) = number of possible connections for which data were available; total (column) = 2(N2-N) for ipsilateral (connection from a region to itself ignored) + 2(N2) for contralateral.

[3] Number of connections present (bilateral): data available (column) = connections reported to exist; extrapolated (column) = estimated total number of connections that exist in the full network, extrapolated from the number of possible connections for which data were available, according to the completeness of the dataset (this assumes a representative sampling of connection data in the literature). Note that the number of connections reported to exist includes reports of axons-of-passage that were assigned a conservative connection strength of weak (see text for details).

[4] Percentage of possible connections for which data were available in the literature.

[5] Network connection density, expressed as a percentage: the number of connections reported as present with data available, divided by the number of possible connections. The same percentage applies to extrapolated connections present divided by the total number of connections possible.

[6] Number of reports that were entered for all possible connections in the network: This number includes reports of possible connections for which no data were available, in addition to reports for which data were available. For right and left brain sides, reports were collated for one side only (numbers doubled for the bilateral network).

**Fig. 2.** A summary of major connection data measures for the bilateral adult rat brain.

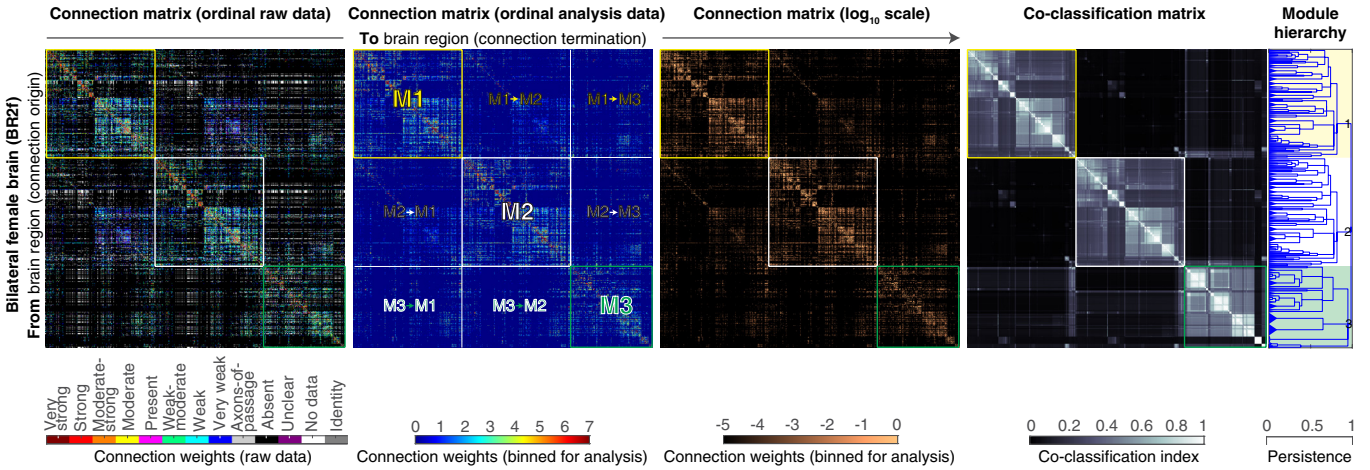


**Fig. 3.** Bilateral intrabrain connectomes for adult female rat (BR2f). Directed and weighted monosynaptic connection matrices with gray matter region sequence in a module arrangement derived from multiresolution consensus cluster (MRCC) analysis (right column). Collated data are represented by descriptive terms with ordinal weight values (left column) and then binned for analysis (second column). For binning, "present" was assigned a "moderate" value, axons-of-passage was converted to "weak," and "unclear" was converted to "absent." This matrix was then converted to log-weighted values (third column) for computation. MRCC analysis of the binned, log-weighted connection data generated a coclassification matrix (fourth column), also represented as a nested hierarchy tree or dendrogram (right column). Coclassification refers to how consistently a given node pair (present or absent connection) affiliates with the same network module across all partitions captured by MRCC analysis. The linearly scaled coclassification index gives a range between 0 (no coclassification at any partitioning resolution) and 1 (perfect coclassification across all partitioning resolutions). Individual MRCC runs consisted of 1.5 million uniformly sampled partitions. In an MRCC hierarchy, branch length represents a distance between where the branch was created and where it either splits or reaches the end of the hierarchy (a terminal branch). This length may be interpreted as the branch's persistence across the entire hierarchy such that dominant solutions (branches more resistant to splitting) have longer branches and fleeting or unstable solutions have shorter branches. For MRCC analysis, three tiny region pairs (nucleus of lateral olfactory dorsal cap, parapyramidal nucleus, obscurus raphe nucleus) were eliminated from the dataset because they failed to achieve symmetric placement using a rationale and method described previously (12). All solutions plotted in the module hierarchy survive statistical testing with a significance level of $\alpha = 0.05$. For region (row and column) identity and additional details, see Datasets S3 and S4, where the underlying connection data and module organization are easy to explore.

and then global, features of BR2 neural network organization. For local approach methodology, we used multiresolution consensus cluster analysis (9, 29), which samples all levels of cluster partitioning resolution in contrast to nonconsensus methods requiring supervised cluster number and/or partitioning resolution selection. MRCC analysis hypothesizes relationships between neural elements based on the fundamental assumptions that strongly interconnected region clusters form stable modules or subsystems with unique functional properties, and that module members have stronger mutual connections within the module than with other modules. The unsupervised, data-driven results distinguish modules of various sizes that are arranged in a matrix and accompanying nested hierarchy (dendrogram), together representing a compact description of all modules and all interactions between them (Fig. 3, *Right* two columns; Datasets S3 and S4, Layer H). MRCC analysis yields a predictive model of (or hypothesis about) network organization that can be tested experimentally.

The MRCC-defined female hierarchy (BR2f) is considered first. It has 289 modules arranged in a 73-level hierarchy, with three first-order modules and 157 terminal modules (Dataset S4, Layer D). As an interpretive framework, this MRCC structural hierarchy for BR2f (Fig. 3, *Right* column) was annotated provisionally and conservatively (Dataset S4, Layer D) with the most general and obvious functional correlates at the region level, as documented in the references for connection reports in Dataset S2. For example, the retina to suprachiasmatic nucleus (SCN) connection transmits entraining luminance information to the endogenous circadian clock, the dorsal lateral geniculate nucleus connection transmits retinal information for visual perception, and the retina to olivary pretectal nucleus connection participates in the pupillary light reflex. This approach was followed in our earlier investigation of intrinsic forebrain (13), midbrain (14), rostral sector (15), rhombicbrain/intermediate sector (16), and spinal cord/caudal sector (17) connections.

**Top–Down Module Analysis Reveals Distinct Brain Modules for Behavioral Control and Execution.** Top–down analysis of the MRCC hierarchy affords a big picture perspective aiding comprehension and interpretation of its nested modules. There are just three first-order modules in the BR2f hierarchy; two (M1 and M2) are predominantly unilateral and form a bilaterally symmetrical pair, whereas the third (M3) is unitary and bilateral. This relatively simple solution is not necessarily expected; for example, we found that the cerebral cortex displays six first-order modules (8), both pons and medulla display 5 first-order modules (16), and forebrain (13) and cerebellum (16) display the minimum, two first-order modules.

Two interrelated approaches suggest a structure–function hypothesis for the three first-order modules: the possible functional significance of their second- and third-order branches, and their spatial distribution in the brain. The functional significance of this first-order module configuration is suggested in the annotated BR2f MRCC hierarchy, which is too large to display in journal page format (Dataset S4, Level D). As outlined in Fig. 4, M1 (and mirror image M2) has three second-order branches. M1.1 is associated with learned-voluntary behavior control (accompanied by cognition and affect), and includes most corticothalamic interactions, classical basal ganglia, and locus ceruleus; its main fiber tract is the predominantly crossed lateral forebrain bundle system of comparative neuroanatomy (13, 30). In contrast, M1.2 is associated with instinctive-survival behavior control, homeostasis, and biorhythms. It includes predominantly the basal endbrain, hypothalamus, and periaqueductal gray; its main fiber tract is the predominantly uncrossed medial forebrain bundle system (13, 30). M1.3 includes retinal projections to the superior colliculus and related regions, but with the notable exception of the dorsal lateral geniculate nucleus (in M1.1). The latter result suggests high-level modular brain network differentiation of retinal neural information streams associated with visual perception and optic reflex control.

**Brain structure-function modules/subsystems (upper levels)**

**Module 1 (M1): Behavior control (rostral sector: forebrain-midbrain)**
- 1.1 Learned behavior control with cognition & affect (lateral forebrain system)
  - 1.1.1 Somatic-gustatory-olfactory perception with motor output
  - 1.1.2 Visual & auditory perception
  - 1.1.3 Cortical executive functions
- 1.2 Instinctive behavior control with homeostasis & biorhythms (medial forebrain system)
  - 1.2.1 Agonistic-reproductive-locomotor behavior control
  - 1.2.2 Eating-drinking-reproductive behavior interactions with homeostatic-biorhythm integration
  - 1.2.3 Vagus nerve control
  - 1.2.4 Reward & drive
- 1.3 Luminance detection & optic reflexes

**Module 2 (M2): Mirror-image of M1**

**Module 3 (M3): Behavior execution (intermediate sector: rhombicbrain)**
- 3.1 Cerebellar eye-body movements (vestibular & somatic sensory inputs, pontine reticular nucleus)
  - 3.1.1 Left side: cerebellar eye-body movements
  - 3.1.2 Right side: cerebellar eye-body movements
- 3.2 Reticular formation face-body movements (taste & visceral sensory-motor, medullary reticular formation)
  - 3.2.1 Left side: reticular face-body movements
  - 3.2.2 Right side: reticular face-body movements
- 3.3 Brainstem auditory
- 3.4 Locomotion (vestibular & hippocampal influences)

**Fig. 4.** A top–down structure–function interpretation of the MRCC module hierarchy; for lower levels see Dataset S4, Layer D.

Overall, the results suggest that M1 and mirror image M2 play a major role in learned and instinctive behavior control, and that, in a complementary way, bilateral M3 is involved primarily with behavior execution and reflex integration (Fig. 4). M3 has four bilateral second-order branches. M3.1 is involved primarily with cerebellar influences on coordinating eye-body movements, related mainly to vestibular and somatic sensory inputs. M3.2 is involved primarily with medullary reticular formation influences on coordinating sensory-motor reflexes, related mainly to taste and somatic-visceral sensory inputs. The remaining two M3 second-order branches are small; one (M3.3) consists of brainstem auditory regions, and the other (M3.4) may be related to locomotor activity; among its most prominent members are the dorsal tegmental area and lateral mammillary nucleus, the medial habenula and interpeduncular nucleus, and efferent vestibular nuclei.

Visual inspection (Fig. 5*A* and Dataset S5) shows that the spatial distribution of regions in the BR2f network first-order modules (M1–M3) is mostly segregated in an easily recognizable pattern. Regions forming M1–M2 predominate in the rostral sector (forebrain-midbrain), whereas regions forming M3 predominate in the caudal sector (rhombicbrain), with modest overlap concentrated in the midbrain-pons. Furthermore, M1 occupies one side of the rostral sector—except for 3/285 contralateral regions associated with visual (retina and parabigeminal nucleus) and somatosensory (cuneate nucleus) inputs—M2 is centered in the opposite rostral sector side, and unitary M3 is bilaterally symmetrical and centered in the intermediate sector. Notably, the overall division of M1–M2 into a dorsolateral system related to learned behavior control and a ventromedial system related to instinctive behavior control, homeostasis, and biorhythms was predicted by the appearance of these general motifs in our earlier investigation of intrinsic forebrain (13) and rostral sector (15) modular network organization.

**Bottom–Up Brain Module Analysis Drives Formulation of Testable Hypotheses.** Bottom–up analysis provides the most granular view of network modular organization. This approach is particularly useful for generating strong testable hypotheses because the 157 terminal modules are experimentally tractable region sets assumed to be functionally related—there are on average five robustly interconnected regions per terminal module (range: 2 to 30 regions). Three practical hypotheses (13) are illustrated in Fig. 6 for a branch of BR2f associated with visual and auditory perception. The first hypothesis is that module members with poorly understood functional attributes share overall functional attributes of the entire module. The second hypothesis is that if a parent module has two or more children with apparently distinct functional properties, then the parent module integrates those two or more functional properties. And the third hypothesis is that if a parent module has two children, one with clear functional properties and the other without, then the parent module displays the known and unknown functions of its children.

The application of these three hypotheses is illustrated in Fig. 6 for a branch of BR2f associated with visual and auditory perception. Module (M1.1.2) has two children, one of which (M1.1.2.1) forms a terminal module with a set of 11 regions. Assigning broad functional significance to M1.1.2.1 is straightforward: It includes the dorsal lateral geniculate nucleus and all 10 visual cortical areas identified in the rat. Note that retinorecipient regions other than the dorsal lateral geniculate nucleus, such as the SCH (circadian rhythm generation) and superior colliculus (predominantly optic reflexes) are not associated with M1.1.2.1.

The second branch of M1.1.2 is associated broadly with auditory perception, but in contrast to terminal module M1.1.2.1, this module (M1.1.2.2) displays a branching pattern with five terminal modules. The first terminal module here (M1.1.2.2.1.1.1, a seventh-order branch in the overall hierarchy) is also relatively easy to interpret. It contains two parts of the medial geniculate complex and all four auditory cortical areas identified in the rat. Inclusion of temporal association areas (TEa) in this module suggests the hypothesis that in the rat, this cortical area's predominant functional role is associated with auditory perception. The second terminal module here (M1.1.2.2.1.1.2) contains three midbrain auditory "relay" regions including two parts of the inferior colliculus. Note that these two end branches are children of a module (M1.1.2.2.1.1) that can now reasonably be labeled "auditory perception." The third terminal module here (M1.1.2.2.1.2) notably contains the posterior parietal and ectorhinal areas of cerebral cortex and the thalamic lateral posterior nucleus. The fact that M1.1.2.2.1.2 and the preceding M1.1.2.2.1.1 are children of parent module M1.1.2.2.1 suggests that M1.1.2.2.1.2 is also associated most prominently with auditory perception, though perhaps more in an "association" role. The fourth and fifth terminal modules here also contain regions associated broadly with auditory perception. The notable inclusion here of what has been identified as the supplemental somatosensory area (SSs) suggests the testable hypothesis that in the rat, this cortical area may play a greater role in auditory perception than in somatosensory perception.

This example shows that the MRCC hierarchy displays expected and unexpected results suggesting well-grounded testable hypotheses. The general configuration of the third-order branch used as an example here—M1.1.2, associated most clearly with visual and auditory perception—was observed in MRCC analyses of endbrain (9), forebrain (13), and rostral sector (15) neural networks.

**Connections between Brain Modules.** The MRCC analysis just considered displays all identified modules in a nested hierarchical arrangement (Fig. 3 and Dataset S4, Layer D) but does not indicate the organization of weaker connections between modules, which are clear in the MRCC matrix itself (Fig. 3, *Second* column; Datasets S3 and S4, Layers C–H) and are quantified in Movie S1. For BR2f it is instructive to examine the weighted connection density (WCD) of interactions between the three first-order modules,

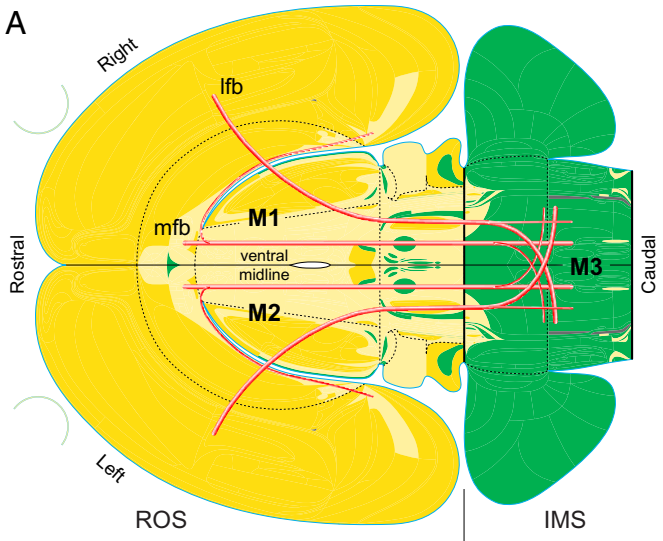


| | CNU | CTX | HY | TH | MB | P | CB | MY |
|---|---|---|---|---|---|---|---|---|
| M1-2: 570 regions | 88 | 152 | 128 | 88 | 66 | 38 | 0 | 10 |
| M3: 214 regions | 2 | 0 | 2 | 4 | 28 | 48 | 38 | 92 |
| M1-2: 100% | | | 91.6% | | | | 8.4% | |
| M3: 100% | | | 16.8% | | | | 83.2% | |
| M1-2: 100% | | 80.0% forebrain | | | 11.6% | 6.7% | 1.8% | |
| M3: 100% | | 3.7% forebrain | | | 13.0% | 22.4% | 60.8% | |

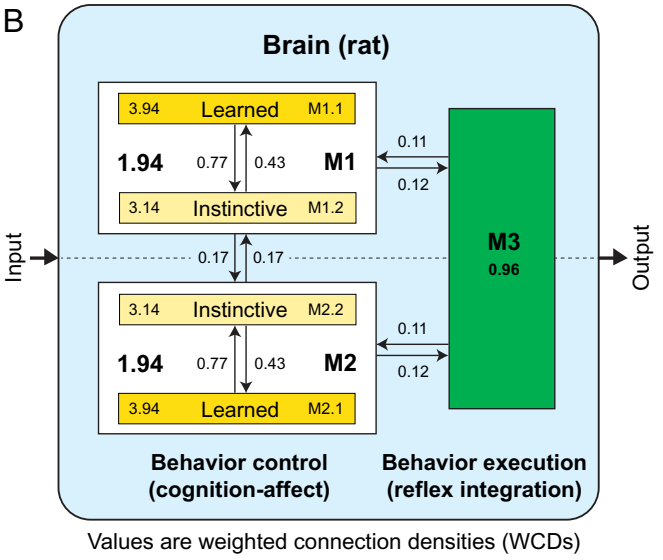


**Fig. 5.** Spatial distribution and block wiring diagram of prominent upper-level BR2f modules. (*A*) A flatmap of the adult rat brain representing the spatial distribution of first-order and select second-order BR2f modules (M): M1 and M2 (yellow) form a mirror-image pair and M3 (green) is unitary and bilaterally symmetrical. The main fiber system of M1.1–M2.1 (darker yellow) is the predominantly crossed lateral forebrain bundle system (lfb), whereas the main fiber system of M1.2–M2.2 (lighter yellow) is the predominantly uncrossed medial forebrain bundle system (mfb). Tabulated below the flatmap is the distribution and proportion of gray matter regions in each brain division for M1–M3. For labeled divisions on a flatmap see Fig. 1 *B* and *C*; for a zoomable flatmap with all regions labeled see Dataset S5. Three tiny regions excluded from MRCC analysis are shaded dark gray (nucleus of lateral olfactory tract dorsal cap, parapyramidal nucleus, obscurus raphe nucleus). (*B*) A quantitative block wiring diagram for connections between the upper-level modules shown in (*A*). Numbers refer to the weighted connection density (WCD; aggregate log-weighted connection strength/total number of possible connections, ×100; individual values in Dataset S3) for intrinsic module connections and for connections between modules. According to the MRCC algorithm, WCD values are always greater within than between modules. For simplicity, the small M1.3 (luminance detection and optic reflexes) is not shown.

compared to the WCDs of interactions within the modules themselves (Fig. 5*B*). The WCD measure suggests that intrinsic connections of M1–M3 are an order of magnitude stronger than connections between them, that intrinsic connections of M1–M2 are about twice as strong as those for M3, and that the intrinsic connections of M1.1 and M1.2 (and mirror image M2.1 and M2.2) are about twice as strong as those for the parent module. Also note that the effects of M1.1 (learned behavior) on M1.2 (instinctive behavior) are almost twice as strong as the reciprocal effects. How this intrabrain network fits within the larger context of the nervous system as a whole, and nervous system interactions with the rest of the body, remains to be determined.

**Global Intrabrain Network Attributes.** After considering the BR2f neural network's hierarchical modular arrangement, the next step involved computing and analyzing four basic attributes associated with global network integration that transcend local module boundaries: region centrality, hubs, rich club, and small world (22). The first attribute, region centrality, captures the relative importance of regions within a network (Dataset S6). Hubs are the second attribute, derived from multiple region centrality measures, and they indicate the most central regions that may facilitate global integrative processes, and/or play critical compensatory roles when the network is compromised (22). Hub identification was based on aggregated rankings across four region centrality measures (degree, strength, betweenness, and closeness), after ranking each region on each metric (Dataset S6). An aggregate "hub score" was determined for each region by summing the number of centrality metrics for which each region appeared in the top 20% (6). Using this criterion, 42 hubs (21 right–left region pairs) were identified in the BR2f network.

The spatial distribution of BR2f hubs is striking: all of them are found in the mirror-image pair (M1–M2) centered in the brain's rostral sector, and each of the three second-order branches of M1 (and mirror-image partner M2) also contain hubs. Furthermore, the hubs are rather broadly distributed; of the 63 terminal modules in M1, 16 have one hub, one has two hubs, and one has 3 hubs (for their identity and module assignment see Dataset S4, layer D; and Dataset S5).

The results of centrality analysis for all regions are given in Dataset S6. For example, the five BR2f regions with the highest degree centrality (the most input and output connections) are, in descending order, the ventral tegmental area, posterior hypothalamic nucleus, locus ceruleus, dorsal raphe nucleus, and tuberomammillary nucleus (Dataset S6*B*). The number of input and output connections (Dataset S6*A*) is roughly similar for the ventral tegmental area and posterior hypothalamic nucleus, whereas the number of outputs is considerably greater than the number of inputs for the tuberomammillary nucleus, suggesting that it is predominantly a "sender" region. In contrast, the retrorubral region is predominantly a "receiver" region; it has considerably more input connections than output connections.

A third global network attribute—the rich club—is defined as a core set of individually highly connected regions (high degree) that are also mutually highly interconnected (31), more so than expected by chance. Rich club organization has previously been found in many brain networks from different species, including some, but not all, subdivisions of the rat brain. Two statistically significant sets of regions forming a rich club were identified in the BR2f network. (Fig. 7). The larger set contains 100 regions (50 left–right region pairs) spanning modules 1, 2, and 3. The smaller set has the largest normalized rich-club index and it is

convenient to focus on its 28 regions (14 right–left region pairs), all of which are in module 1 (and mirror image module 2). In essence, this BR2f "richest club" forms a secondary or derived network with broadly distributed regions superimposed on, and presumably coordinating, the underlying modular arrangement. At upper hierarchy levels (Fig. 4 and Dataset S5), the instinctive behavior control module (M1.2) dominates; it has 10 richest-club members in nine terminal modules, whereas the learned behavior control module (M1.1) has two members, and the optic reflex module (M1.3) also has two members.

Small world is the fourth global network attribute; it occurs in networks with highly clustered regions connected by short paths (32, 33) and may indicate efficient communication in terms of energy cost (34). Small-world attributes of the BR2f network are among the strongest we have computed for the 19 bilateral subconnectomes forming smaller components within the BR2f network (Fig. 8 *A* and *B*). Only the endbrain, forebrain, and rostral sector subnetworks display stronger small-world attributes—and the former two are components of the latter, where M1 and M2 are concentrated, and where most hubs and rich-club members in the BR2f neural network are located. At the other extreme, the bilateral intermediate sector/rhombicbrain, thalamic, cerebellar, medullary, and spinal cord subnetworks display no small-world attributes; whereas the bilateral cerebral cortex subnetwork displays intermediate small-world attributes (Fig. 8*A*); interestingly, the unilateral (association) cerebral cortical network shows only modest small-world attributes (CTX1 in Fig. 8*B*). Note that in every case, addition of commissural connections to unilateral connections increased clustering but not necessarily the small-world index (SWI) because path length results were mixed.

**Region-Level Computational Network Manipulations Reveal Local and Global Brain Network Effects.** After examining BR2f neural network modular and global features, we modeled the impact of focal computational manipulations—to simulate structural lesions or circadian rhythms—on local and global network organization. First, each of the 392 right–left BR2f region pairs was individually lesioned computationally by setting its input–output connections to zero, computing its MRCC coclassification matrix, and determining differences with the intact brain coclassification matrix. The results confirmed for the brain three previously identified factors, based on more limited datasets (13, 15), contributing to the magnitude and spread of focal lesion effects on global network organization: region centrality (Fig. 9 *A* and *B* and Dataset S6), module identity (see Dataset S4, Layer L for retina as an exemplar of lesion-effect "stripes" of multiregion sets associated with module boundaries), and pattern of region input–output connections (Dataset S4, Layer L for retina as an exemplar).

For each brain region, the data were also used to plot lesion impact in terms of magnitude and spread (Fig. 9*C* and Dataset S7).

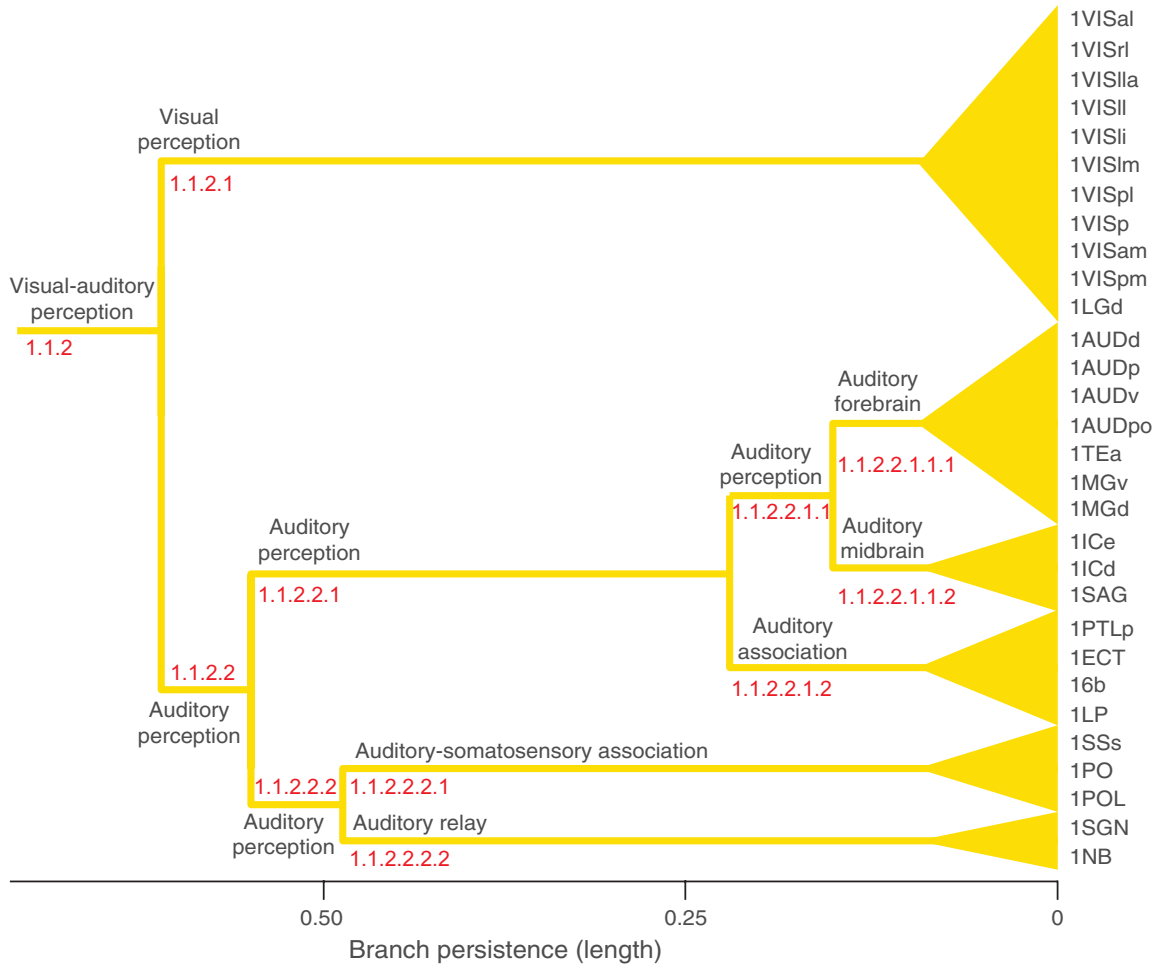


**Fig. 6.** Bottom–up structure–function interpretation of a representative part of the BR2f MRCC module hierarchy. General functional associations are indicated with concise phrasing (derived from longer descriptions associated with the complete hierarchy in Dataset S4, Layer D); alternate and more specific interpretations may be formulated by examining the complete set of regions for each module (numbered in red). In MRCC hierarchies, child branch order, and region order in terminal modules, are random, and may be rearranged for clarity without altering network structure. For region abbreviations see Dataset S1; the "1" prefix for region abbreviations refers to one side (left or right) of the brain.

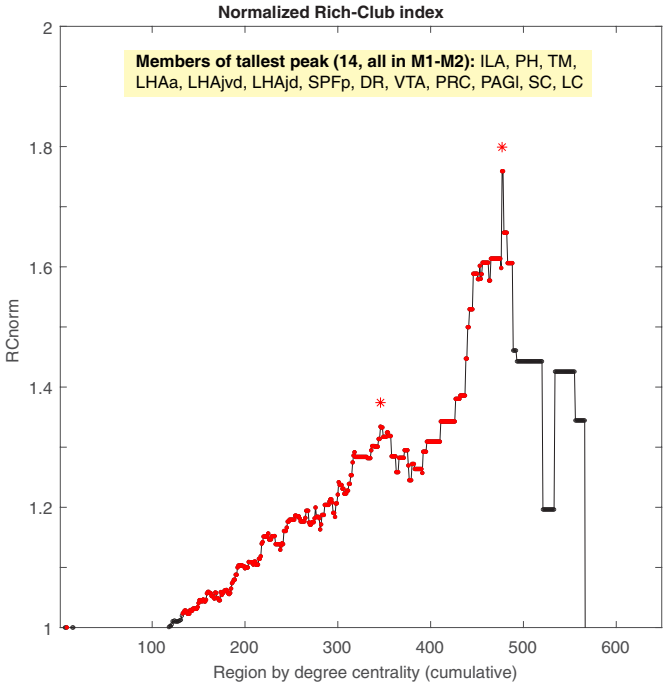


**Fig. 7.** Detecting the most prominent BR2f network rich-club members. The normalized rich-club index (RCnorm) is computed as the ratio between the density of connections between a set of regions found in the empirical network, divided by the mean density found in a null model preserving node degrees but randomizing global network organization. A value greater than 1 indicates higher density than expected by chance. All 790 regions are arranged in order of their degree centrality metric, and each distinct set of regions with degrees greater than the value indicated on the *x* axis is statistically tested (red dots indicate statistically significant values). Two peaks indicated by a red asterisk (*) are most prominent and statistically significant (with $P = 0$ for both peaks). For the highest peak (*Right*), the connection density of its 28 members (one member of the 28 right–left pairs is listed above) most exceeds the expected (null) mean (=1); that is, the set has the greatest RCnorm (plotted on the *y* axis). On the *x* axis, a degree value indicates regions with that degree or higher; thus, the right peak is a subset of the left peak. For region abbreviations see Dataset S1.

Among the 10 regions having the greatest impact in each category, three stand out as occurring in both lists (Fig. 9*C*): the lateral entorhinal area (implicated in Alzheimer's disease tauopathy) has the broadest effect throughout the brain network, the dorsal medullary reticular nucleus (implicated in coordinating head and body reflexes) has by far the greatest magnitude effect on brain network organization, and the magnocellular dentate nucleus (a main route for cerebellar hemisphere output) is intermediate between the other two.

Finally, the data were used to calculate for each network region-pair (possible connection) a "vulnerability score"—simply, how many of the 392 region-pair lesions produce a statistically significant change in coclassification index for a region-pair of interest (Fig. 9*D*; for a completely labeled matrix see Dataset S4, Layers J and K). Two features are obvious. First, as exemplified by the mirror-image module pair, ipsilateral region pairs (M1 or M2) are more vulnerable than contralateral region pairs (M1→M2 or M2→M1). And second, region-pair lesion vulnerability tends to occur more frequently in discontinuous stripes representing multiregion sets aligning with specific modular boundaries. For example, one strong set (Fig. 9 *D, -a,a*) is centered in two adjacent modules, one associated with reward and drive (M1.2.4) and the other associated with luminance detection and optic reflexes (M1.3) (Fig. 4). In contrast, a weaker, broader set (Fig. 9 *D, -b,b*) lies within M3.1.1, which is associated with vestibular and somatosensory influences on cerebellar eye-body movement control (Fig. 4). Horizontal stripes denote output connections and corresponding vertical stripes denote input connections of relevant region-pairs and modules.

***A circadian rhythm.*** The SCH acts as the brain's circadian clock by generating an endogenous circadian rhythm of neuronal firing activity (35). We simulated dynamic changes in SCH output connection weights that mimic circadian changes in neuronal activity and used changes in module affiliation or coherence (coclassification index) as a proxy for dynamic changes, having confirmed (36) that this measure provides a good approximation of neuronal activity covariance structure (Dataset S4, Layer O). As predicted from its relatively modest lesion impact score (Fig. 9*C*, red dot), major cyclic changes in SCH coclassification score were restricted to four right–left module pairs (Movie S2 and Dataset S4, Layer O) containing a) the SCH itself; b) the thalamic rostral reuniens nucleus, which receives a projection from SCH and is closely associated with the hippocampal ventral subiculum; c) the retina, intergeniculate leaflet, and terminal nuclei of accessory optic tract, and d) pretectal nuclei controlling lens and pupil reflexes (Dataset S4, Layer D). The retina, which transmits entraining luminance information directly to the SCH (35), also projects to 33 other region-pairs in the brain (Dataset S3). Computational retina lesions, as predicted from its relatively high impact score (Fig. 9*C*), display much broader effects on BR2f network organization (Dataset S4, Layer L) than SCH manipulations.

**Brain Network Sexual Dimorphisms.** Two right–left pairs of sexually dimorphic unilateral connections involved in controlling ovulation and other reproductive functions have been clearly identified in the rat (37); they arise in the bed nuclei of terminal stria principal part (BSTpr), a cerebral nuclei region, and terminate in the anteroventral periventricular nucleus (AVPV) and ventral premammillary nucleus (PMv), regions in the hypothalamus. The BSTpr→AVPV connection is ~6× heavier in males than females, and the BSTpr→PMv connection is ~4× heavier in males. Thus, 4/623,310 possible connections in the BR2 neural network are clearly sexually dimorphic, requiring separate analysis of each connection matrix.

Comparison of the BR2f and BR2m MRCC hierarchies identified four regions that switched terminal module identity, with 3 of them restricted to Module 1.2.1 (M1.2.1, and mirror image M2.2.1). This switching resulted in the reordering of nine sequential hierarchy terminal modules in females and males (Fig. 10). The most obvious functional correlates of the affected regions are the expression of reproductive and agonistic behaviors and the expression of various circadian rhythms (Dataset S4, Layer D). The fourth region, the anterior pretectal nucleus, switched from a terminal module in M1–M2 containing the superior colliculus, to a terminal module in M3 containing other pretectal nuclei; all affected regions here appear to play a role in various optic reflexes. Curiously, this anterior pretectal switch from M1–M2 to M3 could result in the switch of auditory brainstem M3.2 (which has the greatest branch persistence of any terminal module in the hierarchy) to primary M4 (Dataset S4, Layers D, P, and Q) in males. This change from three to four primary modules occurred in 4/5 MRCC analyses (1.5 million samples/run) for male and 1/5 MRCC analyses (same sampling) for female.

**Extent of Crossed Intrabrain Connections.** Available data indicate that the rat brain neural network's right and left halves are bilaterally symmetrical with respect to axonal connections between regions. It is therefore of interest to compare ipsilateral connections and connections crossing from one side to the other (contralateral/crossed connections) for the brain and its

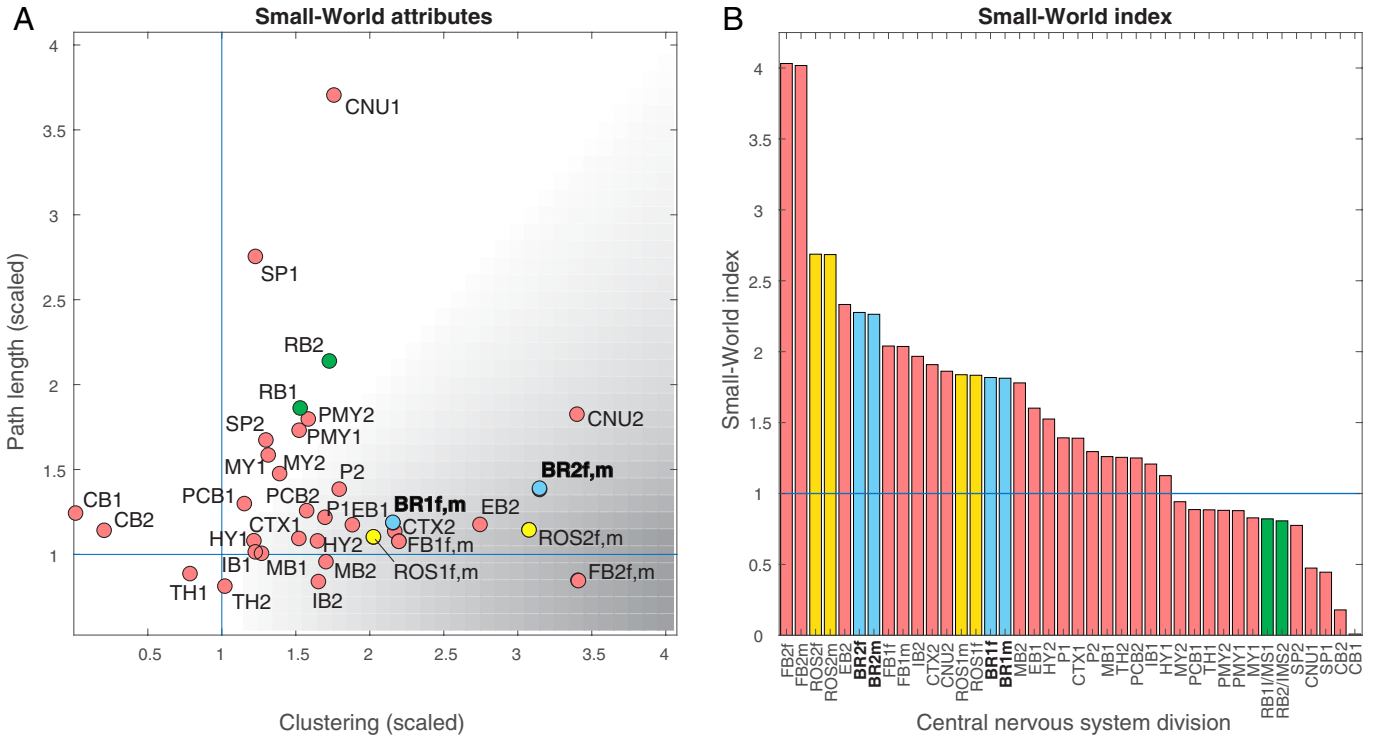


**Fig. 8.** Small-world analyses of the rat brain and main CNS divisions. (*A*) A plot of small-world properties for BR2 compared with properties for other major CNS divisions (prefixes 1, 2 indicate unilateral and bilateral networks; suffixes f, m indicate female, male). Small-world networks have two main properties: highly clustered (densely interconnected) regions and relatively short paths between two regions. Clustering is computed as the mean of all weighted-directed clustering coefficients, and path length is computed as the mean of the weighted path lengths between all region pairs. Both metrics are scaled by the corresponding measures' medians from 1,000 degree-preserving randomized networks. The ratio between scaled clustering and scaled path length is the SWI (33). For a network to display small-world attributes, its SWI should be >1, with a high (scaling ≫ 1) clustering index and a short (scaling near 1) path length. For comparison, values are also plotted for our previously reported subconnectomes (7–17). (*B*) Data from (*A*) were used to calculate a SWI (scaled clustering/scaled path length), which was then used to rank order the CNS divisions. Bar colors correspond to those in (*A*). For abbreviations see Fig. 1*C* and: PCB, pons-cerebellum; PMY, pons-medulla.

major divisions (*SI Appendix*, Table S1), as done previously for the cerebral cortex (8). Major findings are that a) contralateral connections account for 31% of all intrabrain connections, b) there are 64× more heterotopic than homotopic contralateral connections (11,016:172), c) 44% of all possible homotopic contralateral connections exist, d) 41% of ipsilateral connections have a matching contralateral connection, and e) only 0.6% (720) of contralateral projections have no matching ipsilateral

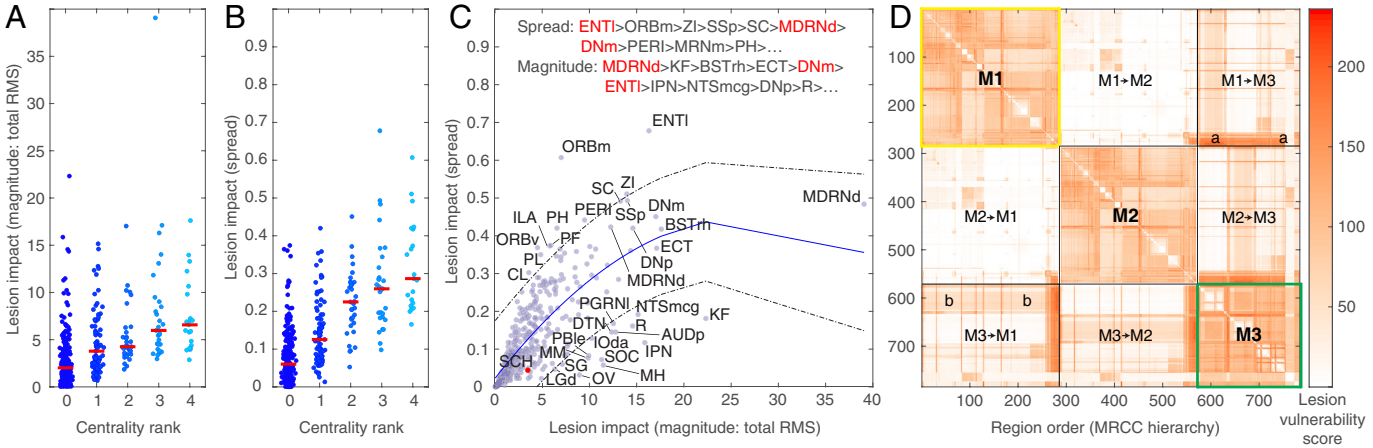


**Fig. 9.** Effects of focal computational lesions on the BR2f network. In *A* and *B*, each of the 392 MRCC matrix mirror-image region-pairs (blue dots) was lesioned and total impact was measured in two ways. (*A*) The sum of RMS changes (magnitude) in coclassification module-affiliation score (index) for all region pairs (possible connections) was plotted against the lesioned region's centrality rank (hub) score. The median lesion impact (red bars) increased with each increase in centrality rank although the range of effects showed considerable overlap. (*B*) Total lesion impact was also assessed by determining how many elements of the matrix were significantly affected (distribution/spread). Significance threshold was set to the 99.9th percentile of differences between identical runs on the BR2f matrix. As in *A*, mean lesion impact (red bars) significantly increased with each increase in centrality rank but with considerable overlap. (*C*) For all region pairs, a plot of the relationship between two lesion impact measures: total RMS (*A*) and distribution/spread (*B*). A second-degree polynomial fit with 95% CI is displayed and distinguishes some regions with unusually broad distribution of lesion changes (*Above*) and other regions with considerable total lesion impact restricted to a small part of the matrix (*Below*). Text at top lists 10 ranks for region pairs with respectively the greatest lesion spread and impact; red type identifies regions in both lists. For region abbreviations see Dataset S1. (*D*) Region-pair vulnerability as measured by the number of focal regions producing a change in coclassification index for the region pair (lesion vulnerability score). Discontinuous stripes (for example, *a,a-b,b*) are discussed in the text. For a matrix with labeled regions and modules (M1–M3) see Dataset S4, Layers C, D, and J.

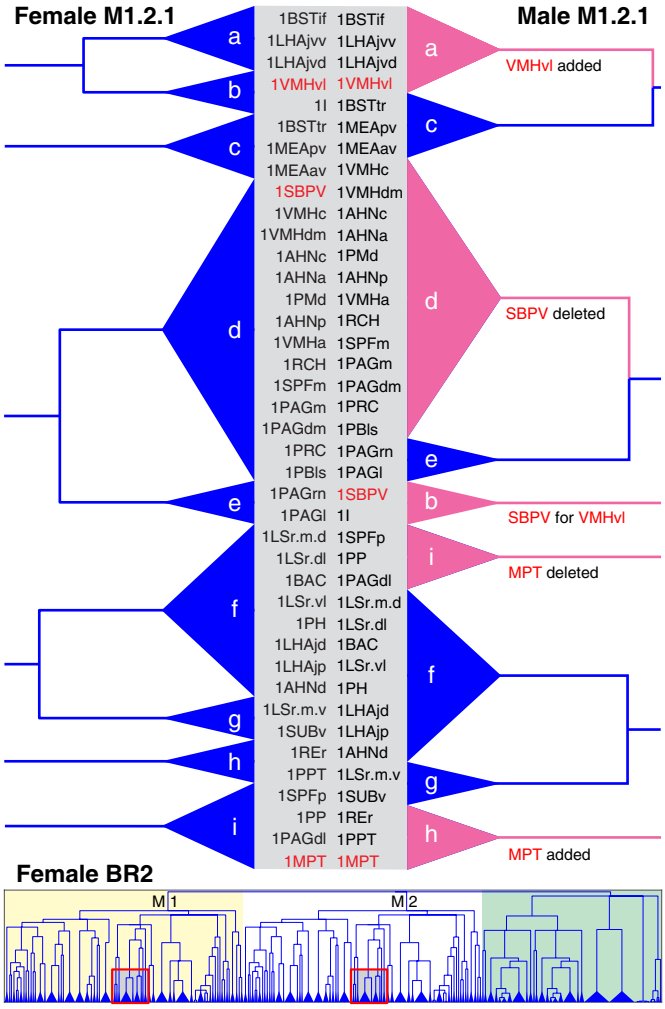


**Fig. 10.** In Module 1 (M1, and mirror image M2), sexual dimorphisms in the brain MRCC hierarchy resulting from sexually dimorphic connections are restricted to Module 1.2.1 (M1.2.1, and mirror image M2.2.1; red boxes at bottom). This dimorphism is reflected in module reassignment of three regions (red abbreviations), reordering a segment of nine consecutive terminal modules (a–i), which also reorders some parts of the associated hierarchy. As in Fig. 6, the order of regions within a terminal module have been rearranged for clarity. For a complete male hierarchy and matrices see Dataset S4, Layers P and Q).

connection. These values differ considerably for individual brain divisions (*SI Appendix*, Table S1).

## Discussion

There are four main outcomes of the work reported here. First, a curated database with just over a million connection report rows and 18 main data and metadata columns was created for the adult female and male rat brains. Second, the database was used to establish general boundary conditions for the magnitude of species-specific, genetically hard-wired connectivity within the intrabrain neural network (about 77,000 connections between 790 regions, for a network density of about 12%). Third, network science tools applied to the brain neural network suggest a structure–function model organized as a nested hierarchy of interconnected modules—which are defined as region clusters that have denser connections within than between modules, and as such are hypothesized to play specialized functional roles. And fourth, simulated focal manipulations (complete, graded, or cyclical changes in region connection weights) of the global network point the way toward a predictive and dynamic structural connectomics.

Before discussing the results further, it is important to note two broad limitations of our approach, which have been addressed elsewhere (16, 17) and for brevity are only summarized here. The first limitation is incomplete data. At the region to region macroconnectome level (20, 38) we have chosen, where data for the rat brain are by far most complete, about 6% of possible connections have not been examined in the rat, and data validity varies considerably. Thus, the underlying connection data will presumably become more complete and valid with time, requiring careful versioning of underlying databases (8); we merely provide version 1.0. And of course, the macroconnectome level does not consider neuron types at the mesoconnectome level and individual neurons at the microconnectome level—or the accompanying axon collateralization and biophysical measures associated with them. What our results do provide is a testable model that can be improved over time with a wide range of structural and functional data. The second broad limitation is that the network properties described here apply only to intrinsic brain connections. When connections with other nervous system parts are added, specifically with spinal cord, peripheral nervous system, and pituitary, network properties of brain regions may be expected to change (16).

From the top–down, most general perspective, MRCC analysis of the female rat brain yields a model with three interconnected, first-order modules in a nested structure–function hierarchy. One mirror-image pair of first-order modules is associated primarily with behavior control, whereas a bilateral single module (or perhaps a double module in males) is associated primarily with behavior execution. Remarkably, the behavior control modules show a pronounced spatial localization to the CNS rostral sector (forebrain and midbrain), whereas the behavior execution module is localized predominantly to the CNS intermediate sector (cerebellum, pons, and medulla). And notably, the behavior control modules each have two main second-order modules, one related to instinctive behavior control, and the other related to learned or voluntary behavior control. This simple neural network model, with many nested levels of modularity farther down the hierarchy, is derived from unsupervised cluster analysis of a relatively complete, uniformly sampled dataset. In contrast, there is no clear consensus in current ways to enumerate brain systems (39–42), based on the supervised assessment of criteria such as classical ontologies, research tradition, or putative behavioral and psychological processes.

Instead, our three-module neural network model of a mammalian brain (Fig. 5) is supported by evolutionary, embryological, and physiological evidence (for reviews see refs. 16, and 43) indicating that the chordate CNS has three fundamental, rostrocaudally arranged sectors. Our results suggest that a mirror-image pair of first-order modules—a set of densely interconnected gray matter regions associated with behavior control—is centered in the rostral sector, whereas a single (or possibly double, in the male) bilateral first-order module associated with behavior execution is centered in the intermediate sector. This evidence suggests a close biological relationship between neural tube primary vesicle embryogenesis (Fig. 1*A*) and the genetic program that subsequently assembles the species-specific connectivity pattern of the adult rat brain (Fig. 5). Whether a generally comparable connectivity pattern associated with neural tube vesicle differentiation applies to all chordates will require a great deal more evidence. However, a synaptic-level structural connectome (44) for an ascidian nervous system (45) does appear to share certain basic features. Specifically, the larva of *Ciona intestinalis* (a primitive chordate class in the subphylum Tunicata) displays three modules in the rostral sector and one module, called the motor ganglion, in the intermediate sector; other modules include the caudal sector (spinal cord of vertebrates) and peripheral nervous system. How connectome

organization of invertebrate cerebral ganglia (46, 47) relates to a chordate basic plan also remains to be determined.

We have also begun to explore here and elsewhere (13, 15) the effects on global network organization of simulated focal changes in connection weight, including computation deletion ("lesion") of inputs and outputs, inputs alone, or outputs alone, and cyclic changes in connection weight, an approach pioneered empirically in *Caenorhabditis elegans* (48). The results suggest the extent to which each region/node in the network is vulnerable to focal lesions elsewhere, the magnitude and spread of focal lesion effects, and factors contributing to effects of focal manipulation on global network organization. One unexpected factor is the tendency for focal connection manipulation effects to aggregate as multiregion sets within module boundaries, that is, affecting modular relations as a whole and appearing as stripes in the coclassification matrix. This finding suggests that normal and pathological local changes in the brain neural network are to some extent "bottled up" within modules, echoing the long-established principle that pathological changes in the body may be cell-, tissue-, or organ-specific. The finding also suggests that modular structure may confer redundancy, such that if the function of one region in a module is lost or compromised, it may be at least partly compensated by activity in one or more other regions of the module. This intermodular spread of focal lesion effects may harness inherent network mechanisms ensuring robustness and compensation (1).

The network analysis carried out in this paper is deliberately simple, focusing on basic aspects of modular architecture and prioritizing compatibility with our earlier studies of rat brain divisions. The datasets published with this article afford other researchers the opportunity to explore these data with additional computational tools, including different clustering algorithms, network metrics, and null models. Especially worthwhile targets are more general community detection methodologies including weighted stochastic block models (49, 50), directed motifs (51, 52), communication models (53), and more conservative null models that preserve spatial embedding (54). The brain's connection matrix, as furnished here, may also serve as a basis for future work exploring dynamic simulations of whole brain activity.

In conclusion, this study presents a draft of a complete mammalian brain interregional connectome, with comprehensive data coverage for all anatomical divisions, supported by a foundational database. The resulting annotated structure–function network model and analyses reveal features of architecture and organization that can provide a robust guide for future experimentation and manipulation designed to reveal structure–function relationships. The value of a more expansive future model, where the brain network is considered in relation to the entire nervous system, and beyond to the other body systems it senses and partly controls, is readily appreciated. Such a holistic model's connection matrix has been called a neurome (6), and its databases may be used as a framework for knowledge management systems underlying applications analogous to Google Maps (38). Furthermore, this study illustrates how structural connectomes may serve as predictive dynamic structural connectivity models for the elaboration of strong, testable hypotheses about biological mechanisms underlying the emergent properties of mind and behavior by the healthy, diseased, or injured nervous system.

## Materials and Methods

The connectome database was expertly collated from the neuroanatomical literature (ref. 13 and *SI Appendix*, *Materials and Methods*). Cluster analysis was performed using the multiresolution consensus cluster method (9, 29). Module analysis and display was performed as described in the text.

**Data, Materials, and Software Availability.** Connection report data and metadata are in a Microsoft Excel spreadsheet (Dataset S2), as are data from the reports used for connection matrices (Dataset S3). Searchable connection report data are freely available at The Neurome Project (https://sites.google.com/view/the-neurome-project/home). Network analyses were done on the BR2 connection matrix (Dataset S3; see first worksheet "Key" for a description of the workbook contents), with tools collected in the Brain Connectivity Toolbox (https://sites.google.com/site/bctnet/). Previously published data were used for this work [Some values in the connection matrix were previously published in our PNAS papers; they are clearly identified in Fig. 1 legend and in *SI Appendix* (they are from refs. 15, and 16)]. All other data are included in the manuscript and/or supporting information.

Author affiliations: [a]Department of Biological Sciences, University of Southern California, Los Angeles, CA 90089; [b]Indiana University Network Science Institute, Indiana University, Bloomington, IN 47405; and [c]Department of Psychological and Brain Sciences, Indiana University, Bloomington, IN 47405

1. O. Sporns, G. Tononi, R. Kötter, The human connectome: A structural description of the human brain. *PLoS Comput. Biol.* **1**, e42 (2005).
2. D. H. Meadows, *Thinking in Systems: A Primer* (Chelsea Green, 2008).
3. J. W. Lichtman, J. R. Sanes, Ome sweet ome: What can the genome tell us about the connectome? *Curr. Opin. Neurobiol.* **18**, 346–353 (2008).
4. L. W. Swanson, What is the brain? *Trends Neurosci.* **23**, 519–527 (2000).
5. M. Bota, H.-W. Dong, L. W. Swanson, From gene networks to neural networks. *Nat. Neurosci.* **6**, 795–799 (2003).
6. M. Bota, O. Sporns, L. W. Swanson, Architecture of the cerebral cortical association connectome underlying cognition. *Proc. Natl. Acad. Sci. U.S.A.* **112**, E2093–E2101 (2015).
7. L. W. Swanson, O. Sporns, J. D. Hahn, Network architecture of the cerebral nuclei (basal ganglia) association and commissural connectome. *Proc. Natl. Acad. Sci. U.S.A.* **113**, E5972–E5981 (2016).
8. L. W. Swanson, J. D. Hahn, O. Sporns, Organizing principles for the cerebral cortex network of commissural and association connections. *Proc. Natl. Acad. Sci. U.S.A.* **114**, E9692–E9701 (2017).
9. L. W. Swanson, J. D. Hahn, L. G. S. Jeub, S. Fortunato, O. Sporns, Subsystem organization of axonal connections within and between the right and left cerebral cortex and cerebral nuclei (endbrain). *Proc. Natl. Acad. Sci. U.S.A.* **115**, E6910–E6919 (2018).
10. L. W. Swanson, O. Sporns, J. D. Hahn, The network organization of rat intrathalamic macroconnections and a comparison with other forebrain divisions. *Proc. Natl. Acad. Sci. U.S.A.* **116**, 13661–13669 (2019).
11. J. D. Hahn, O. Sporns, A. G. Watts, L. W. Swanson, Macroscale network architecture of the hypothalamus. *Proc. Natl. Acad. Sci. U.S.A.* **116**, E8018–E8027 (2019).
12. L. W. Swanson, O. Sporns, J. D. Hahn, The network architecture of rat intrinsic interbrain (diencephalic) macroconnections. *Proc. Natl. Acad. Sci. U.S.A.* **116**, 26991–27000 (2019).
13. L. W. Swanson, J. D. Hahn, O. Sporns, Structure-function subsystem models of female and male forebrain networks integrating cognition, affect, behavior, and bodily functions. *Proc. Natl. Acad. Sci. U.S.A.* **117**, 31470–31481 (2020).
14. L. W. Swanson, J. D. Hahn, O. Sporns, Subsystem macroarchitecture of the intrinsic midbrain neural network and its tectal and tegmental subnetworks. *Proc. Natl. Acad. Sci. U.S.A.* **118**, e2101869118 (2021).
15. L. W. Swanson, J. D. Hahn, O. Sporns, Structure-function subsystem model and computational lesions of the central nervous system's rostral sector (forebrain and midbrain). *Proc. Natl. Acad. Sci. U.S.A.* **119**, e2210931119 (2022).
16. L. W. Swanson, J. D. Hahn, O. Sporns, Intrinsic circuitry of the rhombicbrain (central nervous system's intermediate sector) in a mammal. *Proc. Natl. Acad. Sci. U.S.A.* **120**, e2313997120 (2023).
17. L. W. Swanson, J. D. Hahn, O. Sporns, Network architecture of intrinsic connectivity in a mammalian spinal cord (the central nervous system's caudal sector). *Proc. Natl. Acad. Sci. U.S.A.* **121**, e2320953121 (2024).
18. L. W. Swanson, M. Bota, Foundational model of structural connectivity in the nervous system with a schema for wiring diagrams, connectome, and basic plan architecture. *Proc. Natl. Acad. Sci. U.S.A.* **107**, 20610–20617 (2010).
19. R. A. Brown, L. W. Swanson, Neural systems language: A formal modeling language for the systematic description, unambiguous communication, and automated digital curation of neural connectivity. *J. Comp. Neurol.* **521**, 2889–2906 (2013).
20. L. W. Swanson, J. W. Lichtman, From Cajal to connectome and beyond. *Annu. Rev. Neurosci.* **39**, 197–216 (2016).
21. M. Breakspear, C. J. Stam, Dynamics of a neural system with a multiscale architecture. *Philos. Trans. R. Soc. B.* **360**, 1051–1074 (2005).
22. O. Sporns, *Networks of the Brain* (MIT Press, 2011).
23. J. D. Hahn *et al.*, An open access mouse brain flatmap and upgraded rat and human brain flatmaps based on current reference atlases. *J. Comp. Neurol.* **529**, 576–594 (2021).
24. L. Luo, *Principles of Neurobiology* (CRC Press/Garland Science, ed. 2, 2020).
25. J. E. Knox, High-resolution data-driven model of the mouse connectome. *Netw. Neurosci.* **3**, 217–236 (2018).
26. L. Coletta *et al.*, Network structure of the mouse brain connectome with voxel resolution. *Sci. Adv.* **6**, eabb7187 (2020).

27. L. W. Swanson, Brain maps 4.0–Structure of the rat brain: An open access atlas with global nervous system nomenclature ontology and flatmaps. *J. Comp. Neurol.* **526**, 935–943 (2018).
28. L. W. Swanson, *Neuroanatomical Terminology: A Lexicon of Classical Origins and Historical Foundations* (Oxford University Press, 2016).
29. L. G. S. Jeub, O. Sporns, S. Fortunato, Multiresolution consensus clustering in networks. *Sci. Rep.* **8**, 3259 (2018).
30. L. W. Swanson, *Brain Maps: Structure of the Rat Brain* (Elsevier, 1992).
31. V. Colizza, A. Flammini, M. A. Serrano, A. Vespignani, Detecting rich-club ordering in complex networks. *Nat. Phys.* **2**, 110–115 (2006).
32. D. J. Watts, S. H. Strogatz, Collective dynamics of "small-world" networks. *Nature* **393**, 440–442 (1998).
33. M. D. Humphries, K. Gurney, Network "small-world-ness": A quantitative method for determining canonical network equivalence. *PLoS ONE* **3**, e0002051 (2008).
34. E. Bullmore, O. Sporns, The economy of brain network organization. *Nat. Rev. Neurosci.* **13**, 336–349 (2012).
35. M. U. Gillette *et al.*, Intrinsic neuronal rhythms in the suprachiasmatic nuclei and their adjustment. *Ciba Found. Symp.* **183**, 134–153 (1995).
36. M. Pope, M. Fukushima, R. F. Betzel, O. Sporns, Modular origins of high-amplitude cofluctuations in fine-scale functional connectivity dynamics. *Proc. Natl. Acad. Sci. U.S.A.* **118**, e2109380118 (2021).
37. G. Gu, A. Cornea, R. B. Simerly, Sexual differentiation of projections from the principal nucleus of the bed nuclei of the stria terminalis. *J. Comp. Neurol.* **460**, 542–562 (2003).
38. R. A. Brown, L. W. Swanson, Golgi: Interactive online brain mapping. *Front. Neuroinf.* **9**, 1–16 (2015).
39. R. Nieuwenhuys, J. Voogd, C. van Huijzen, *The Human Central Nervous System* (Springer, ed. 4, 2008).
40. L. W. Swanson, *Brain Architecture: Understanding the Basic Plan* (Oxford University Press, ed. 2, 2012).
41. G. Paxinos, *The Rat Nervous System* (Elsevier, ed. 4, 2015).
42. E. Kandel, J. D. Koester, S. H. Mack, S. A. Siegelbaum, *Principles of Neural Science* (McGraw Hill, ed. 6, 2021).
43. R. Nieuwenhuys, Deuterostome brains: Synopsis and commentary. *Brain Res. Bull.* **57**, 257–270 (2002).
44. K. Ryan, Z. Lu, I. A. Meinertzhagen, The CNS connectome of a tadpole larva of *Ciona intestinalis* (L.) highlights sidedness in the brain of a chordate sibling. *eLife* **5**, e16962 (2016).
45. D. Nicol, I. A. Meinertzhagen, Cell counts and maps in the larval central nervous system of the ascidian *Ciona intestinalis* (L.). *J. Comp. Neurol.* **309**, 415–429 (1991).
46. S. J. Cooke *et al.*, Whole-animal connectomes of both *Caenorhabditis elegans* sexes. *Nature* **571**, 63–71 (2019).
47. M. Winding *et al.*, The connectome of an insect brain. *Science* **379**, eadd9330 (2023).
48. E. K. Towlson *et al.*, *Caenorhabditis elegans* and the network control framework–FAQs. *Philos. Trans. R. Soc. B.* **373**, 20170372 (2018).
49. T. P. Peixoto, Nonparametric weighted stochastic block models. *Phys. Rev. E* **97**, 012306 (2018).
50. J. Faskowitz, O. Sporns, Mapping the community structure of the rat cerebral cortex with weighted stochastic block modeling. *Brain Struct. Funct.* **225**, 71–84 (2020).
51. R. Milo *et al.*, Network motifs: Simple building blocks of complex networks. *Science* **298**, 824–827 (2002).
52. J. Faskowitz, R. F. Betzel, O. Sporns, Edges in brain networks: Contributions to models of structure and function. *Network Neurosci.* **6**, 1–28 (2022).
53. C. Seguin, O. Sporns, A. Zalesky, Brain network communication: Concepts models and applications. *Nat. Rev. Neurosci.* **23**, 493–504 (2023).
54. F. Váša, B. Mišić, Null models in network neuroscience. *Nat. Rev. Neurosci.* **23**, 493–504 (2022).